Forcing mechanisms of dielectric barrier discharge plasma actuators at carrier frequency of 625 Hz

M. Kotsonis[a] and S. Ghaemi
Delft University of Technology, Kluyverweg 1, The Netherlands

(Received 8 September 2011; accepted 18 October 2011; published online 1 December 2011)

The forcing behavior of a dielectric barrier discharge (DBD) actuator is investigated experimentally using a time-resolved particle image velocimetry (PIV) system in conjunction with a phase shifting technique. The spatio-temporal evolution of the induced flowfield is accurately captured within one high voltage (HV) cycle allowing the calculation of the instantaneous velocity and acceleration. Additional voltage and current measurements provide the power consumption for each case. Four different applied voltage waveform shapes are independently tested, namely, sine, square, positive sawtooth, and negative sawtooth at fixed applied voltage (10 kV_{pp}) and carrier frequency (625 Hz). The instantaneous flowfields reveal the effect of the plasma forcing during the HV cycle. Sine waveform provides large positive forcing during the *forward stroke*, with minimal but still positive forcing during the *backward stroke*. Square waveform provides strong and concentrated positive and negative forcing at the beginning of the *forward* and *backward stroke*, respectively. Positive sawtooth provides positive but weak forcing during both strokes while the negative sawtooth case produces observable forcing only during the *forward stroke*. Results indicate the inherent importance of negative ions on the force production mechanisms of DBD's. Furthermore, the revealed influence of the waveform shape on the force production can provide guidelines for the design of custom asymmetric waveforms for the improvement of the actuator's performance. © *2011 American Institute of Physics*. [doi:10.1063/1.3664695]

I. INTRODUCTION

Plasma actuators have been the focus of extensive research recently, due to their flow control capabilities. Several concepts and applications have been investigated ranging from separation control[1] to boundary layer control,[2,3] noise reduction[4] and laminar-turbulent transition delay.[5] Detailed reviews on the physics, modeling and applications of this type of actuators are available.[6,7]

This study considers the dielectric barrier discharge (DBD) actuator (Fig. 1). This is the most conventional configuration of plasma actuator with two electrodes. The electrodes are separated by a dielectric layer which prohibits arc forming and allows accumulation of the ionized species in the vicinity of the exposed electrode. Radio frequency (RF) high voltage (HV) is applied to the exposed electrode while the covered electrode is grounded. The HV is typically alternating current (AC) with the most usual waveform being sinusoidal. Due to the large difference in potential between the two electrodes, a strong electric field develops in the vicinity of the actuator. This, in turn, creates a weakly ionized plasma in a small region above the dielectric barrier. The created plasma is generally regarded quasi-neutral and behaves in a typical barrier discharge regime.

The exact mechanism of momentum transfer from the weakly ionized gas to the ambient air is partly unclear. It is widely regarded that collisional processes drive the momentum transfer.[8] This is further supported by an important property of the plasma discharge in air. This states that the frequency of charged species-neutral particles collisions within the plasma region is of the same or larger order of the electrostatic oscillations frequency. This effectively means that the Coulombian forces exerted on the charged particles by the electric field are transferred entirely to the neutral air. Yet the influence of the heavy species to the net momentum transfer and how this affects the direction of the force during the HV cycle is still debated. Early numerical models[9] suggest that during the *forward stroke* (exposed electrode is negative) positive ions are drawn towards the exposed electrode and impart negative momentum to the air. During the *backward stroke* (exposed electrode is positive), the ion movement is reversed and momentum transfer is positive. The net momentum transfer for the entire HV cycle is positive due to the asymmetry in species density between the two strokes. This scenario has been challenged by more recent modeling efforts as well as experimental investigations. Particularly, the consideration of air chemistry and more specifically the existence of negative ions (O^-) in simulations[10,11] is important since in such case, the forcing scenario is completely altered. In models where negative ions are considered, both cycles contribute positively in momentum transfer with the negative half cycle responsible for the majority of the momentum input.

There have been a limited number of experimental investigations on the forcing mechanisms of the actuators. Time-resolved laser Doppler anemometry (LDA) measurements were conducted in quiescent air[12] where the asymmetry between the two half cycles is evident. Large momentum transfer during the negative half cycle was recorded which corresponds with the recent modeling efforts. In another

[a]Author to whom correspondence should be addressed. Electronic mail: m.kotsonis@tudelft.nl.

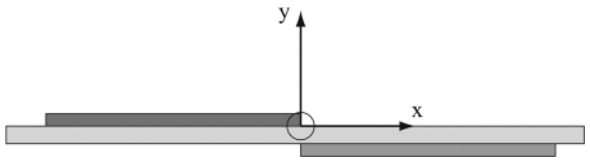

FIG. 1. Schematic of the plasma actuator used in this study. The coordinate system presented here is used throughout this paper.

study,[13] phase locked particle image velocimetry (PIV) measurements are taken which indicate the dominance of the negative cycle in momentum transfer. Using a different technique, Enloe *et al.*[14] and Font *et al.*[15] showed positive momentum transfer during both half cycles.

The current status of experimental research into the forcing mechanisms of the plasma actuator is restricted to either spatial[13] or temporal[12,14] resolution of the flowfield. The experimental investigation in this paper is aimed at the simultaneous spatial and temporal resolution of the induced flowfield from the operation of the plasma actuator within one period of forcing. This information will provide insight into the forcing mechanisms of the actuator and the nature of the momentum transfer process. The results can further be used for comparison and validation of first-principles plasma actuator models as well as optimization of some operating parameters such as the waveform shape for the improvement of the performance of the actuator.

II. EXPERIMENTAL SETUP

A. The actuator

In this investigation, conventional DBD actuators are used, employing thin rectangular copper electrodes made out of self-adhesive copper tape (Fig. 1). The electrodes are 10 mm in length (x direction), with zero horizontal gap. Their thickness is 30 μm including adhesive. The effective spanwise length (z direction) of the electrodes (along which plasma is generated) is 200 mm. The electrodes are separated by two dielectric layers of polyimide Kapton tape. The thickness of each layer is 50.8 μm. The total thickness of the dielectric, including adhesive, is approximately 110 μm. The geometrical properties of the actuator are presented in Table II. The upper electrode is energized using a TREK 20/20C HV amplifier (20 kV, 20 mA) while the lower electrode is kept grounded.

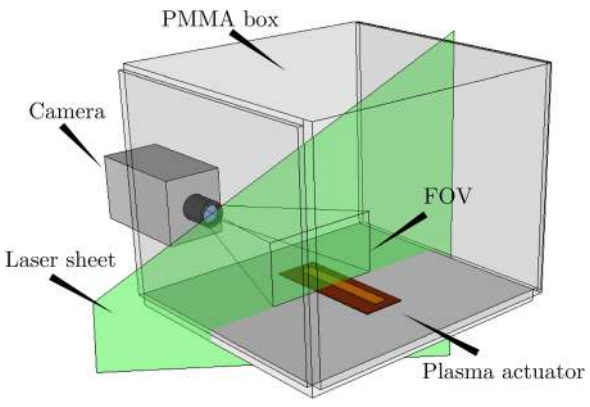

FIG. 2. (Color online) Schematic of the PIV setup for the experimental investigation.

The actuator operation is controlled remotely via a computer workstation where the driving signal is created in LABVIEW software and is sent to the amplifier via a digital/analog (D/A) converter. The amplifier provides direct readings of the output voltage and current through internal measurement probes. While the internal voltage probe gives sufficiently accurate readings the internal current probe has been found to be too slow to resolve high frequency current fluctuations. This is typically the case with discharge currents occurring during plasma actuators operation. To resolve this, a resistance (100 Ω) is placed between the lower electrode and the grounding cable and voltage is measured across it indicating the discharge current.

B. PIV setup

Tests are conducted in a closed box made from Plexiglass (PMMA) to provide optical access. Time-resolved PIV is used in conjunction with a phase shifting technique (described further below) to characterize the flow field in the vicinity of the plasma actuator. A two component PIV configuration has been chosen since the large span of the actuator ensures minimal 3D effects.

The plasma actuator is placed flushed on the bottom of the Plexiglas box. A Photron Fastcam SA1 high speed CMOS camera of 1024×1024 pixels is used to image the field-of-view (FOV). Image acquisition has been conducted at 6 KHz rate in double-frame mode. Time separation of 50 μs has been applied between successive images. A Micro Nikkor 200 mm objective is set at f-stop 4 and is used along with extension tubes in order to achieve 2.1 magnification and a FOV of 9.7×4.7 mm over a cropped sensor of 1024×496 pixels. The air in the Plexiglas box is seeded with olive oil droplets of approximately 1 μm diameter generated by a TSI atomizer. The particles at the mid span of the actuator are illuminated by a light sheet of 2 mm thickness generated by a Quantronix Darwin-Duo laser system with an average output of 80 W at 3 kHz. The images are analyzed using DAVIS 7.4 (Lavision GmbH) by cross-correlating successive images. Final interrogation window size of 16×16 pixels and overlap factor of 75% are used. The interrogation windows are elongated in the wall normal direction using a 4:1 aspect ratio in order to obtain higher spatial resolution. The velocity vectors are returned on a grid of 26×26 vectors per mm^2.

C. Phase shifting technique

For DBD actuators employing thin dielectric layers such as Kapton tape, characteristic carrier frequencies f_{ac} are typically between 0.5 and 10 kHz. This range corresponds directly to the characteristic electrostatic oscillation frequency of the HV signal. As such it is desirable to accurately capture the response of the induced flow within these time scales in order to safely deduce the features of the forcing mechanism. The desired sampling rate of any data acquisition system should at least be one order of magnitude larger than the respective operating frequency for each test case. As

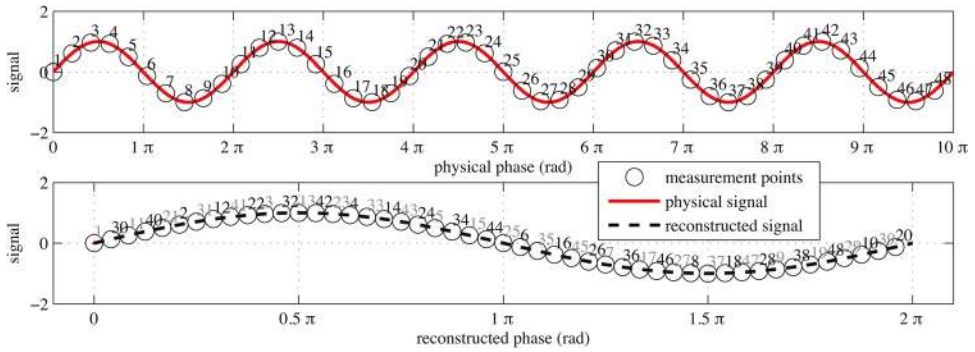

FIG. 3. (Color online) Example of physical and reconstructed signals using the phase shifting technique ($f_{samp} = 6$ kHz, $f_{ac} = 625$ Hz).

already mentioned, it is the goal of this study to simultaneously resolve the spatial and temporal characteristics of the velocity field. The spatial requirement is fulfilled using a 2D PIV system operating at a high optical magnification ($M = 2.1$). The PIV system is capable of high speed acquisition up to 10 kHz limited by the repetition frequency of the laser. Yet this is deemed not sufficient for cases of carrier frequencies larger than 0.5 kHz.

In order to redeem the problem of limited sampling rate, a phase shifting technique is employed to increase the effective sampling frequency of the PIV system. The technique is based on the periodicity of the plasma forcing effect as proved in numerous previous studies.[16,17] More specifically, the sampling rate f_s is kept fixed at 6 kHz while the actuator carrier frequency f_{ac} is chosen such that the ratio $r = f_s/f_{ac}$ is not an integer value. In this manner, the phase of every measured point is slightly shifted between successive actuation signal cycles. This implies that a number of signal cycles c will contain n points with distinct phases which can be combined into a single reconstructed cycle with higher temporal resolution. An example of the phase shifting technique is presented in Fig. 3 with the settings used in the experimental investigation ($f_s = 6$ kHz, $f_{ac} = 625$ Hz). The achieved phenomenal frequency is then given by the product $f_{eff} = n \cdot f_{ac}$.

An overview of the parameters of the phase shifting method as used in this study is presented in Table I. The carrier frequency was chosen such that for every case the final reconstructed signal would consist of 48 points. Although the phenomenal acquisition frequency is 30 kHz the temporal resolution of the system is based on the 50 μs time separation between the PIV image pairs. This translates into a 34% overlap between successive measurement points.

D. Test cases

Due to the advantages in spatio-temporal resolution the selected measurement techniques provide, a series of different waveform shapes is selected for the actuation signal. The selected waveforms include the widely used sinusoidal signal, a square, a sawtooth and a negative sawtooth. All the waveform cases are ran using a fixed carrier frequency $f_{ac} = 625$ Hz and fixed applied voltage $V_{app} = 10$ kV_{pp}. This implies a different power consumption for each waveform which renders the comparison of their performance problematic. As such, no direct performance comparison between the test cases will be currently performed. In contrast the scope of this study is focused on individual forcing mechanisms within each waveform which are treated as individual test cases.

TABLE I. Parameters of the phase shifting technique.

f_{ac} (Hz)	f_s (kHz)	n	c	f_{eff} (kHz)
625	6	48	5	30

A schematic of the different waveforms is presented in Fig. 4. The slight deviations from the ideal shapes are due to the limited slew rate of the HV amplifier (350 V/μs). An overview of the test parameters, including the geometric properties of the actuator, is presented in Table II.

All measurements are taken for continuous operation of the actuator. This implies that the initial transient stage of acceleration from quiescent flow to the fully established wall jet is omitted in order to ensure the temporal periodicity of the flow. For all PIV measurements, 3000 frames are taken from which the necessary number of actuation signal cycles (c, see Table I) is extracted and reconstructed into the enhanced temporal resolution cycle. For every case, a total of 50 reconstructed cycles are gathered and averaged to yield the final flowfield.

III. RESULTS

Prior to the analysis of the temporal characteristics of the reconstructed flowfields, a look at the time averaged velocity fields is taken (Fig. 5). Additionally, the power consumption is calculated since all four waveforms are tested for the same geometrical configuration, applied voltage and carrier frequency. The power consumption is calculated using the integral

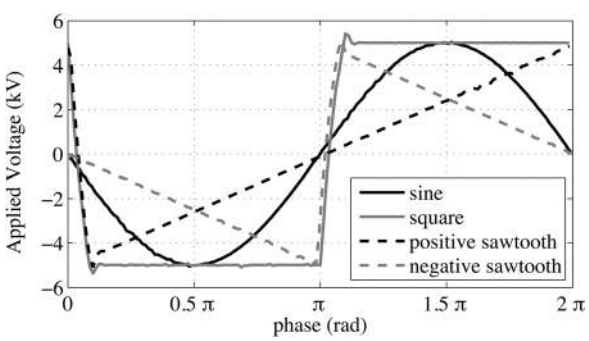

FIG. 4. The HV waveforms tested in this investigation.

TABLE II. Test parameters for the experimental investigation.

Parameter	Value
Upper electrode length (l_u)	10 mm
Lower electrode length (l_l)	10 mm
Dielectric thickness (t_d)	110 μm
Horizontal gap (g)	0 mm
Applied voltage (V_{app})	10 kV_{pp}
Carrier frequency (f_{ac})	625 Hz
Waveform	sine, square, sawtooth, negative sawtooth

$$P = \int_{t_1}^{t_2} |I(t) \cdot V_{app}(t)| dt, \tag{1}$$

where $V_{app}(t)$ is the instantaneous voltage, $I(t)$ is the instantaneous current and $t_2 - t_1$ is a time interval containing an integer number of actuation periods (100). Power consumption for the four tested waveforms is presented in Table III.

The general topology of the flowfield is similar to a typical wall jet. A suction effect is observed slightly downstream of the edge of the exposed electrode ($x = 0$), where flow is entrained towards the wall and then is injected downstream. The sine and square waveforms produce the highest velocities in amplitude. The positive and negative sawtooth actuation is substantially weaker.

The power consumption of the four waveforms reveals additional differences between the waveform shapes. The most energy consuming shape is square while sine requires almost half the power in comparison. Of special interest is the power consumption of the positive and negative sawtooth shapes which is relatively high considering the weak character of the induced flowfield from these two shapes.

Considering the differences in both the induced flowfield and the power consumption for the tested waveforms some remarks must be made here. Care should be taken in

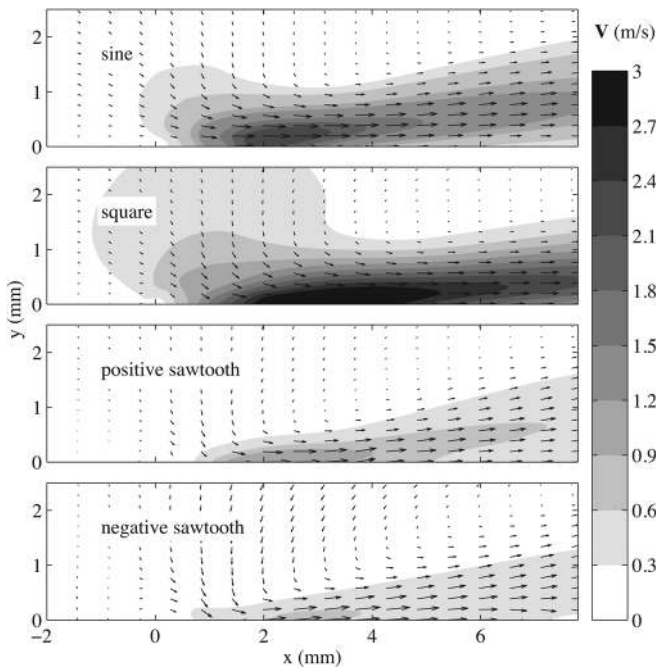

FIG. 5. Average total velocity field corresponding to the four tested waveforms.

TABLE III. Time average power consumtion for the four tested waveforms.

Waveform	Power(W)
Sine	1.8515
Square	3.5413
Positive sawtooth	1.9977
Negative sawtooth	2.9200

comparing the four waveforms. This is due to the differences in power consumption between the four cases. As such, no conclusion on the performance or efficiency as a function of the waveform shape can be obtained by comparing these cases. For instance, in the case of a parametric study for performance improvement through waveform shape manipulation a metric of efficiency should be devised taking into account the strength as well as the power consumption of each shape. In contrast, the scope of this study involves the independent spatio-temporal analysis of the waveforms as standalone cases. An effort to define forcing mechanisms related to the features of each waveform shape is thus undertaken.

In order to obtain a general insight into the underlying scales governing the HV cycle, an initial dimensional analysis is conducted. This is based on the decomposition of the incompressible two-dimensional Navier-Stokes equations based on the available velocity data. More specifically, The NS equations are

$$\frac{\partial \mathbf{V}}{\partial t} + \mathbf{V} \cdot \nabla \mathbf{V} - \nu \nabla^2 \mathbf{V} = -\frac{\nabla p}{\rho} + \frac{\mathbf{F}}{\rho}, \tag{2}$$

where $\mathbf{V} = [u, v]^T$ is the 2D velocity field, $\mathbf{F}$ is the plasma body force field, p is the static pressure, ν is the kinematic viscosity of the fluid and ρ is the density. In the present study, all the left hand side terms of Eq. (2) are available

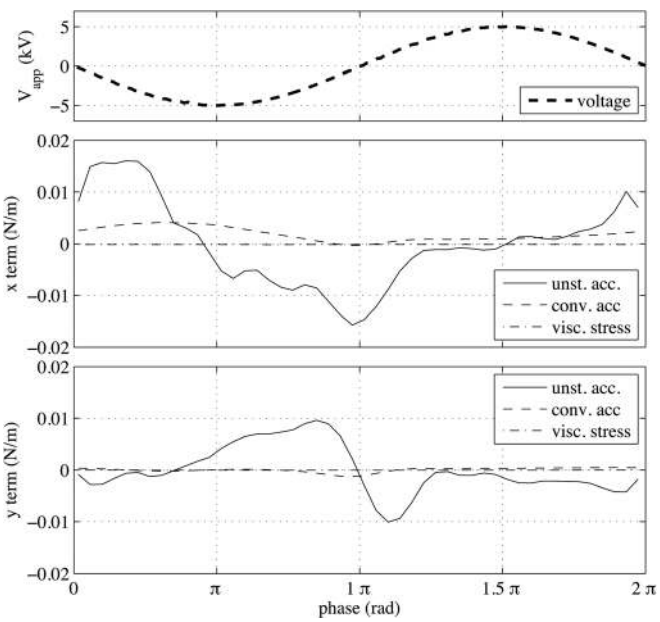

FIG. 6. Dimensional analysis of the measured x and y terms of the Navier-Stokes equations. All terms are integrated over the spatial domain at each time frame.

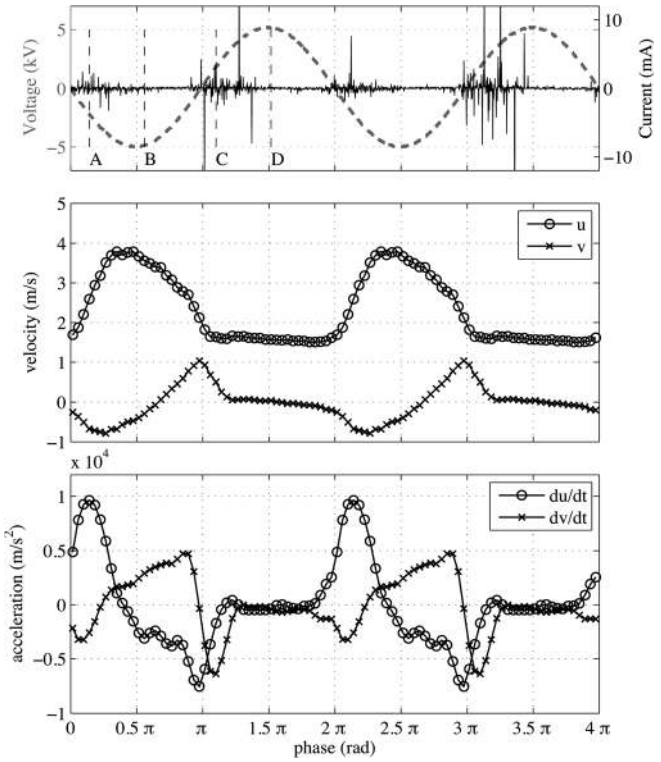

FIG. 7. Temporal evolution of velocity (u, v) and acceleration ($\partial u/\partial t$, $\partial v/\partial t$) during the HV cycle for the sine waveform (values probed at $x = 2$ mm, $y = 0.2$ mm).

through the PIV measurement. On the other hand the pressure gradient and body force terms cannot be uncoupled without erroneous assumptions. This renders the interpretation of the time resolved flowfields more difficult.

Fig. 6 shows the value of the three left hand side terms in Eq. (2) integrated over the spatial domain for the sine waveform case. Similar results are also obtained for the other waveforms. It is apparent that for both the x and y directions, the unsteady acceleration term $\left(\frac{\partial \mathbf{V}}{\partial t}\right)$ dominates the convective acceleration ($\mathbf{V} \cdot \nabla \mathbf{V}$) and the viscous stresses ($-\nu \nabla^2 \mathbf{V}$). This is partly expected as the flow is not confined; it is driven purely by the plasma body force and is largely inviscid. This implies that the pressure gradient might also be small compared to the body force term although no conclusions can be made at this point. For the present study, the dominant term of unsteady acceleration shall be considered as a combined effect of the pressure gradient and the plasma body force.

A. Sine waveform

The first examined waveform is the widely used sinusoidal shape. The majority of experimental[12–14,16] and numerical[10,18] investigations on the DBD forcing mechanisms discuss the sine waveform, albeit for different carrier frequencies and applied voltages. The temporal evolution of velocity and acceleration in the plasma region is presented in Fig. 7 along the measured voltage and current. All flowfield values are probed at approximately the position where the maximum values of velocity are registered ($x = 2$ mm, $y = 0.2$ mm). To be noted here that the reconstructed cycle is presented twice for clarity. Additionally, snapshots of the velocity and acceleration fields are presented in Fig. 8 for four time instants.

For the present study, the first half of the HV cycle (negative exposed electrode) will be denoted as *forward stroke* while the second half of the HV cycle (positive exposed electrode) shall be denoted as *backward stroke*. These terms are retained for all four tested waveforms.

It is evident from the velocity evolution for the sine waveform that the forcing due to the plasma is unsteady and periodic within the HV cycle. Moreover a strong asymmetry exists between the two strokes. The velocity evolution closely resembles results obtained by Forte *et al.*[12] At the initial phases of the *forward stroke* the voltage of the exposed electrode starts to drop (instant A). Simultaneously, the plasma is ignited as indicated by the microdischarges corresponding to current peaks which are registered during the entire negative going portion of the stroke ($0-0.5\pi$). During this period the velocity in the region of the discharge accelerates sharply in the downstream direction. Additionally, a weak vertical component of velocity appears which is directed towards the wall.

At the peak of negative voltage (0.5π), the discharge terminates under the self limiting effect caused by the

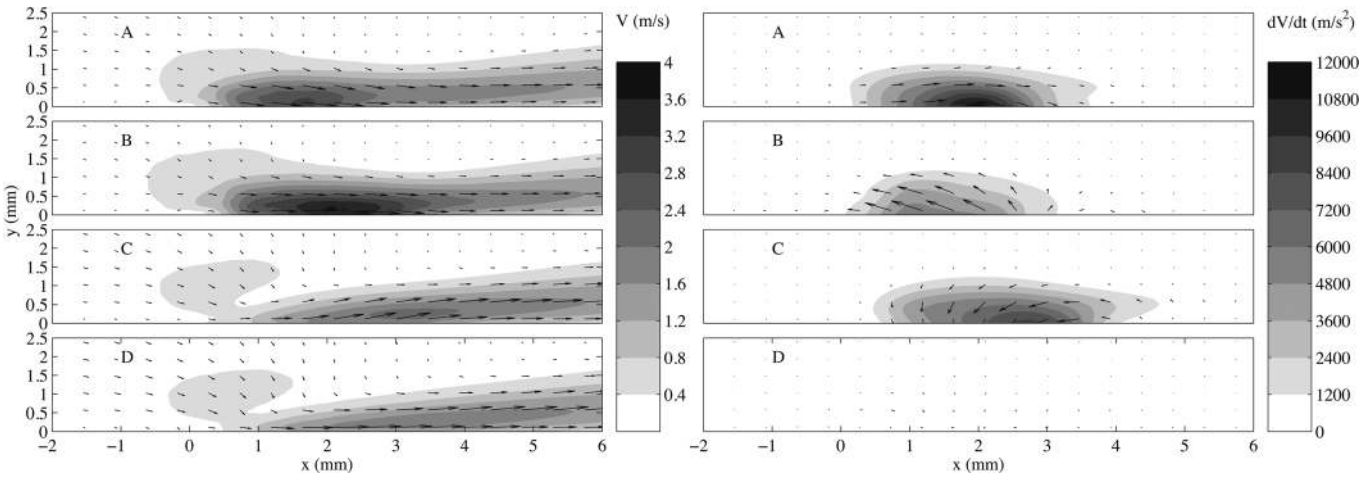

FIG. 8. Snapshots of velocity and acceleration at four instants for the sine waveform. (instants A-D are indicated in Fig. 7).

accumulated charge on the dielectric surface.[10,18,19] The velocity has reached the maximum value and starts decelerating as the voltage increases (instant B). Furthermore, positive vertical acceleration is registered causing fluid to move away from the dielectric wall. It is interesting to note that the slope of change of velocity, and thus, negative acceleration is significantly weaker than the first half of the *forward stroke*. Nevertheless, at 0.9π a sharp increase in negative acceleration is registered.

For the *backward stroke*, no significant change in horizontal velocity is registered (instant C) although the current peaks from π to 1.5π indicate the positive discharge. On the other hand the vertical velocity starts decreasing and drops to zero by 1.2π. This is also indicated by the moderate acceleration vectors towards the wall evident at the snapshot of instant C. For the remainder of the *backward stroke*, both velocity components are constant and respective acceleration drops to zero.

As mentioned earlier, the combined effect of the plasma forcing and the pressure gradient appears to be driving the flowfield acceleration. For the sine waveform, it is apparent that strong momentum addition occurs during the first half of the *forward stroke*. This coincides with the negative discharge as shown by the current peaks. During the negative discharge, negative ions and fast electrons are emitted from the exposed electrode in a series of microdischarges and accumulate on the dielectric surface. The movement of charged particles downstream couples positive momentum to the neutral fluid. For the second half of the *forward stroke*, the flow decelerates mildly, indicating a pressure driven mechanism and absence of any body force. This is further supported by the positive vertical velocity components which indicate an area of high pressure created at the area where the discharge took place in order to fulfill the momentum deficit the sudden disappearance of the body force has created. In contrast, the *backward stroke* appears not to change significantly the flow although a discharge is occurring. This implies the existence of a moderate positive forcing from the plasma. This is enough to keep the flow from decelerating until the next end of the stroke. One event that is currently unclear is the sharp negative acceleration at 0.9π. This might indicate the existence of accumulated negative ions on the dielectric surface which begin to travel upstream as soon as the voltage of the exposed electrode starts increasing. This would imply a small negative body force at the beginning of the *forward stroke*. No definitive conclusion can be made at this point.

Summarizing, the sine waveform appears to produce significant positive forcing during the *forward stroke* with very weak but still positive forcing during the negative stroke. Following the terminology of Corke[7] the action appears to be a PUSH-push effect. This agrees well with the experimental study of Enloe *et al.*[14] where a 97% of momentum addition was registered during the *forward stroke*. Furthermore, the numerical predictions of Boeuf *et al.*[18] are confirmed for the case of low carrier frequency and high voltage amplitude. As they suggest, for these operating conditions, the momentum transfer is dominated by the negative ions movement during the *forward stroke*.

B. Square waveform

The square waveform is tested next. The evolution of velocity and acceleration for the square waveform is shown in Fig. 9 while snapshots of the fields are given in Fig. 10.

The evolution of the flowfield suggests an asymmetry between the two strokes. At the beginning of the *forward stroke* (instant A), the voltage drops sharply. This is accompanied by strong current peaks indicating a, respectively, strong and short negative discharge. During this event, the velocity rises sharply and strong acceleration in the downstream direction is observed. The area of strong acceleration is located well downstream of the exposed electrode with maximum values around $x = 3$ mm. Similarly, the flow is accelerated vertically towards the dielectric surface.

During the remainder of the *forward stroke*, the flow remains at relatively high velocities but constantly decelerates. Respectively, the negative velocity is reduced and approaches zero by the end of the stroke. During this period, no discharge is registered as suggested by the lack of current peaks.

At the beginning of the *forward stroke* (π), the voltage sharply reverts and large current peaks signify the positive discharge. Simultaneously, (instant C) a strong deceleration occurs in the streamwise direction. The slope of velocity change is less than the respective acceleration at the *forward stroke* which is also indicated by the value of the negative acceleration at π. Additionally, the flowfield snapshot at instant C reveals a large, uniformly decelerating area covering almost half the length of the covered electrode. For the

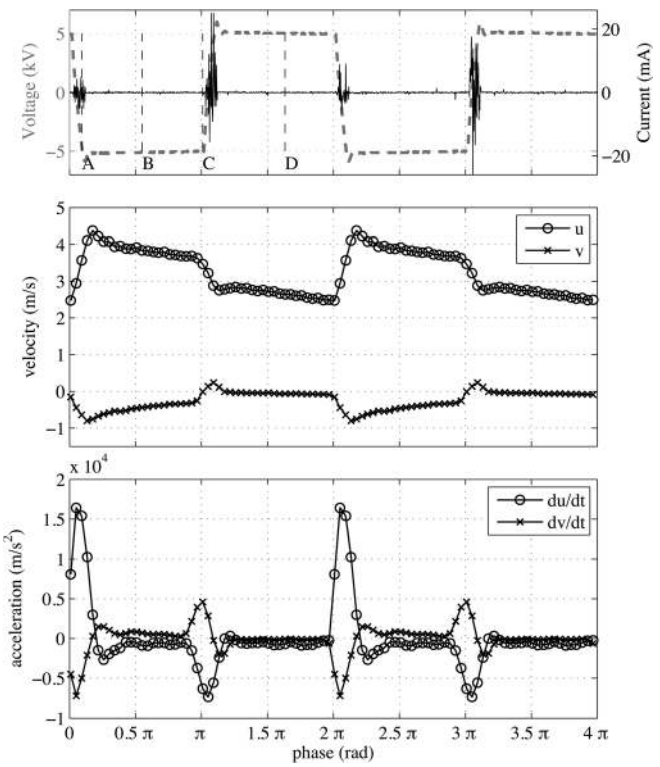

FIG. 9. Temporal evolution of velocity (u, v) and acceleration ($\partial u/\partial t$, $\partial v/\partial t$) during the HV cycle for the square waveform (values probed at $x = 3$ mm, $y = 0.2$ mm).

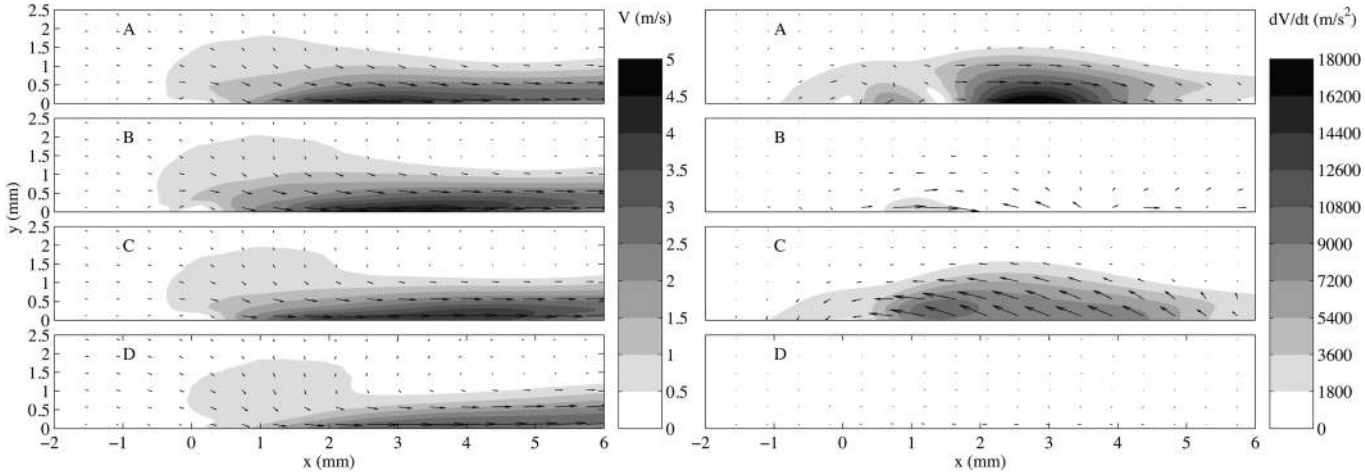

FIG. 10. Snapshots of velocity and acceleration at four instants for the square waveform. (labels A-D are indicated in Fig. 9).

remainder of the *backward stroke* ($1.2\pi-2\pi$), weak deceleration is observed much like the respective period of the *forward stroke*.

The square waveform appears to gather the two active phases in short time periods at 2π and π. Strong events seem to dominate both voltage reversals occurring within the HV cycle. During the voltage drop (2π), the plasma appears to produce strong positive forcing while at the voltage rise (π) the forcing is negative (upstream). During the long periods of flat high voltage, the discharge is quenched and the flow appears to decelerate by pressure gradients alone although. In general, a PUSH-pull event can be identified from the waveform shape.

The concentrated discharge events during the voltage reversal instants appear to be the main mechanism behind the increased power consumption of this waveform. This is due to two simultaneously acting features of the current and voltage evolution, respectively. First, the fast change of voltage from relatively constant positive value to an also relatively constant negative value *compresses* the discharge sequence (avalanche ionization) in a very short time span which in sequence increases its intensity. Second, the instantaneous voltage is theoretically always at peak values for a perfect square shape. This is practically not the case here since the slew rate of the HV amplifier gives a slight slope to the shape. Nevertheless, the instantaneous voltage during the discharge events is generally higher than the respective sine case. The combined effect of both increased voltage and discharge current during the active phases is transferred into the product of these values which in turn produces the relatively high consumed power value.

C. Positive sawtooth waveform

The next tested waveform is the positive sawtooth. Positive and negative sawtooth waveforms have been investigated, albeit in a time averaged way.[19,20] Additionally, the rising and sinking ramp voltage has been investigated numerically as stand alone cases[8] The evolution of velocity and acceleration for the positive sawtooth waveform is shown in Fig. 11 while snapshots of the fields are given in Fig. 12.

At the beginning of the *forward stroke*, the voltage drops sharply with the plasma igniting as indicated by the current peaks. At the same time (instant A), the velocity increases with strong positive acceleration located in a small region downstream the exposed electrode. Additionally, a small but sharp increase of vertical velocity towards the wall is observed.

Shortly, after the acceleration peak the flow starts decelerating at a much lower rate. The deceleration area is located approximately at the same position as the initial acceleration area (instant B). The deceleration of the flow covers the

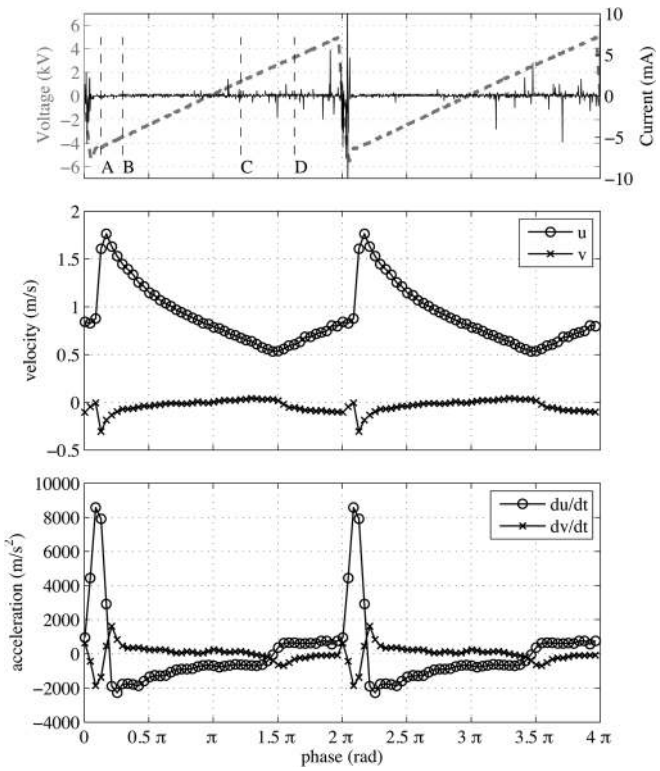

FIG. 11. Temporal evolution of velocity (u, v) and acceleration ($\partial u/\partial t$, $\partial v/\partial t$) during the HV cycle for the positive sawtooth waveform (values probed at $x = 3$ mm, $y = 0.2$ mm).

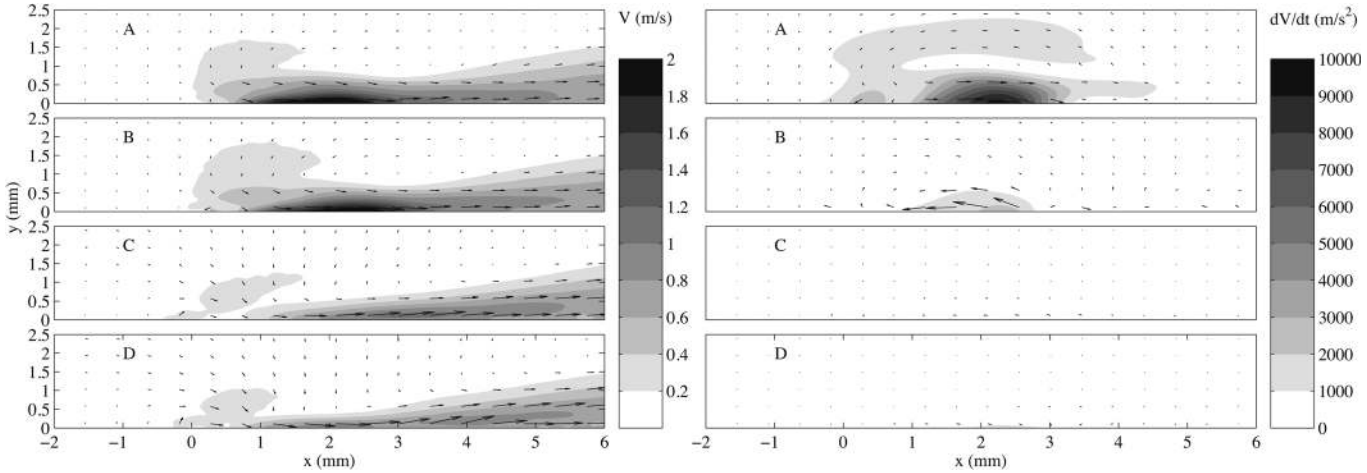

FIG. 12. Snapshots of velocity and acceleration at four instants for the positive sawtooth waveform. (labels A-D are indicated in Fig. 11).

remainder of the *forward stroke* and continues until approximately half the *backward stroke* (1.5π). At this point, the voltage keeps rising and a weak discharge is registered as indicated by the low current peaks (instant D). Furthermore, the flow accelerates weakly again although at a much lower rate compared to the event at the beginning of the *forward stroke*. This weak acceleration continues until 2π where it's superseded by the strong acceleration of the next HV cycle.

The positive sawtooth waveform exhibits an asymmetry between the two strokes. The *forward stroke* produces strong positive forcing during the negative discharge associated with the sharp voltage drop. Subsequently, the flow appears to decelerate on pressure alone until the end of the *forward stroke*. The deceleration continues unaffected, as the *backward stroke* begins and carries on until 1.5π. At this point, weak current peaks are registered indicating the positive discharge. Simultaneously, a moderate positive acceleration occurs signifying weak but still positive forcing from the plasma. The positive waveform appears to produce a PUSH-push effect.

D. Negative sawtooth waveform

The final waveform tested is the negative sawtooth. The evolution of velocity and acceleration for this waveform is shown in Fig. 13 while snapshots of the fields are given in Fig. 14.

At the beginning of the *forward stroke*, the voltage is gradually decreasing (instant A). The flow remains largely unaffected until approximately 0.3π where a moderate positive acceleration is observed in the region of the plasma (instant B) along with weak current peaks indicating the negative discharge. The snapshot of instant B also indicates a large area of negative acceleration above the exposed electrode although the velocity components in the same area are relatively small. At 0.7π the flow starts decelerating smoothly until the end of the *forward stroke*.

During the *backward stroke*, the flow continues to decelerate and seems largely unaffected from the sharp voltage rise, although strong current peaks indicate the occurrence of the positive discharge (instant C). The smooth deceleration continues throughout the *backward stroke*.

The negative sawtooth appears to qualitatively differentiate from the rest of the tested waveforms in the sense that the plasma forcing is visible only during the *forward stroke*. It is also interesting to note that due to the weak nature of the plasma forcing itself, pressure effects seem more pronounced as evident by the large negative acceleration area at instant B. In general, the forcing behavior of the negative sawtooth waveform appears to be a PUSH-none effect.

In the case of the negative sawtooth, the *forward stroke* is responsible for the majority of the momentum input. It is nevertheless interesting to note that this waveform appears not to produce any forcing during the *backward stroke*.

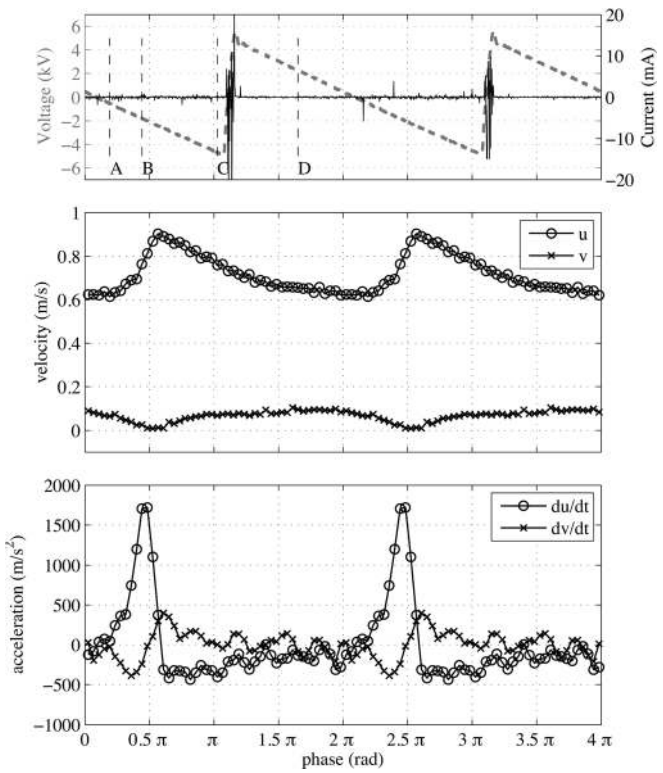

FIG. 13. Temporal evolution of velocity (u, v) and acceleration ($\partial u/\partial t$, $\partial v/\partial t$) during the HV cycle for the negative sawtooth waveform (values probed at $x = 3$ mm, $y = 0.2$ mm).

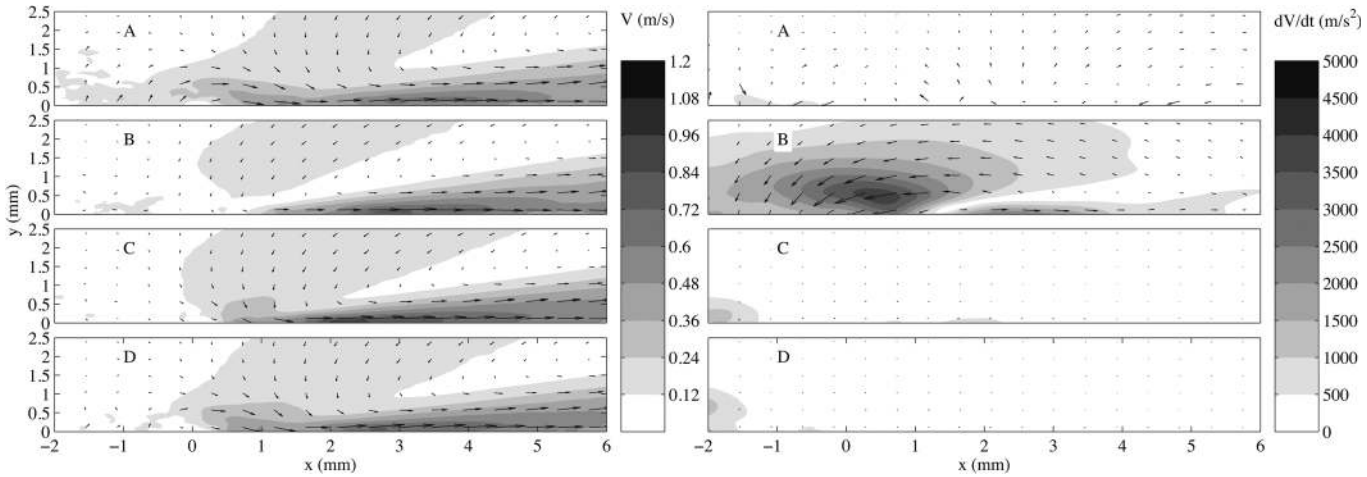

FIG. 14. Snapshots of velocity and acceleration at four instants for the negative sawtooth waveform. (labels A-D are indicated in Fig. 13).

Although the power consumption of the two cases is not the same the general flow topology agrees with previous observations.[20]

IV. DISCUSSION AND CONCLUSIONS

Recent experimental studies indicate that the discharge associated with DBD's is highly asymmetric between the positive and negative half-cycles.[12,19] This has been verified in the present study. Furthermore, four different waveform shapes have been investigated in order to gain insight in the asymmetry and its influence on the plasma forcing.

The sine waveform produces strong acceleration of the flow during the active period of the *forward stroke*. This is associated with the negative discharge where fast electrons and negative ions are emitted from the exposed electrode and accumulated on the dielectric surface[10] coupling momentum to the flow at the same time. On the other hand, the *backward stroke* seems to have little effect in momentum addition although still produces positive force rendering the overall forcing scenario to PUSH-push. Different research groups[14,18] argue that this asymmetry is coupled to the nature of the discharge. For the negative discharge, a large number of microdischarges are responsible for a diffusive and uniform momentum transfer to the neutrals. Contrary, the positive discharge is filamentary and dominated by few strong and concentrated discharges which appear to spatially interact with much less volume of neutral fluid.

The square waveform concentrates the forcing events in short time periods during the voltage reversal at phases π and 2π. These coincide with equally short in time but intense discharge events. Strong acceleration is present during the reversal from positive to negative voltage (beginning of the *forward stroke*). On the other hand, the respective voltage reversal from negative to positive values produces a strong deceleration event which is nevertheless weaker than the respective *forward stroke* forcing. The overall forcing scenario for the square waveform is identified as PUSH-pull.

The positive sawtooth shape presents a concentrated event of positive forcing during the steep voltage drop at the beginning of the *forward stroke*. This is accompanied by strong discharge events. During the linear ramp, voltage rise from π to 2π (*backward stroke*) a sequence of weak discharges is registered during the entire period of the stroke. At the same period, a weak but positive acceleration is registered rendering the overall forcing scenario for this waveform as PUSH-pull.

The negative sawtooth waveform produces positive forcing during the linear ramp from phases 2π to π. On the other hand no perceivable forcing is registered during the sharp voltage rise at the beginning of the *backward stroke* π even though strong discharge current is measured. The overall forcing scenario for the negative sawtooth shape can be identified as PUSH-none.

The results of the present study are suggestive of ways to improve the performance of the plasma actuators. The key seems to be the *forward stroke*, where negative ions are emitted downstream imparting momentum to the flow. While charge equilibrium must remain between the two half cycles, waveforms which present an asymmetry in shape between *forward* and *backward stroke* are expected to enhance the overall performance in terms of forcing strength as well as power consumption.

ACKNOWLEDGMENTS

This work forms part of the CleanEra project initiated by the TU Delft.

[1]M. L. Post and T. C. Corke, AIAA J. **42**(11), 2177 (2004).
[2]J. Huang, T. C. Corke, and F. O. Thomas, AIAA J. **44**(1), 51 (2006).
[3]A. Seraudie, E. Aubert, N. Naude, and J. P. Cambronne, in *3rd AIAA Flow Control Conference* (AIAA, San Francisco, CA, 2006), Vol. 2, pp. 1065–1073.
[4]Y. Li, X. Zhang, and X. Huang, Exp. Fluids **49**(2), 367 (2010).
[5]S. Grundmann and C. Tropea, Exp. Fluids **44**(5), 795 (2008).
[6]E. Moreau, J. Phys. D: Appl. Phys. **40**(3), 605 (2007).
[7]T. C. Corke, C. L. Enloe, and S. P. Wilkinson, Annu. Rev. Fluid Mech. **42**, 505 (2010).
[8]J. P. Boeuf, Y. Lagmich, Th. Callegari, and L. C. Pitchfor, in *45th AIAA Aerospace Sciences Meeting and Exhibit* (AIAA, Reno, NV, 2007), Vol. 4, pp. 2170–2180.
[9]B. Jayaraman, S. Thakur, and W. Shyy, J. Heat Transfer **129**(4), 517 (2007).
[10]A. V. Likhanskii, M. N. Shneider, S. O. MacHeret, and R. B. Miles, J. Appl. Phys. **103**(5) 053305 (2008).

[11]J. P. Boeuf and L. C. Pitchford, J. Appl. Phys. **97**(10), 103307 (2005).
[12]M. Forte, J. Jolibois, J. Pons, E. Moreau, G. Touchard, and M. Cazalens, Exp. Fluids **43**(6), 917 (2007).
[13]W. Kim, H. Do, M. G. Mungal, and M. A. Cappelli, Appl. Phys. Lett. **91**(18), 181501 (2007).
[14]C. L. Enloe, M. G. McHarg, and T. E. McLaughlin, J. Appl. Phys. **103**(7), 073302(2008).
[15]G. I. Font, C. L. Enloe, and T. E. McLaughlin, AIAA J. **48**(9), 1869 (2010).
[16]N. Benard and E. Moreau, J. Phys. D: Appl. Phys. **43**(14), 145201 (2010).
[17]M. Kotsonis, S. Ghaemi, L. Veldhuis, and F. Scarano, J. Phys. D: Appl. Phys. **44**(4), 045204 (2011).
[18]J. P. Boeuf, Y. Lagmich, and L. C. Pitchford, J. Appl. Phys. **106**(2), 023115 (2009).
[19]C. L. Enloe, T. E. McLaughlin, R. D. VanDyken, K. D. Kachner, E. J. Jumper, and T. C. Corke,. AIAA J. **42**(3), 589 (2004).
[20]N. Balcon, N. Benard, Y. Lagmich, J. Boeuf, G. Touchard, and E. Moreau, J. Electrostat. **67**(2–3), 140 (2009).